Geosci. Model Dev., 9, 3671–3684, 2016
www.geosci-model-dev.net/9/3671/2016/
doi:10.5194/gmd-9-3671-2016

Geoscientific Model Development
Open Access
EGU

Computationally efficient air quality forecasting tool: implementation of STOPS v1.5 model into CMAQ v5.0.2 for a prediction of Asian dust

Wonbae Jeon[1], Yunsoo Choi[1], Peter Percell[1], Amir Hossein Souri[1], Chang-Keun Song[2], Soon-Tae Kim[3], and Jhoon Kim[4]

[1]Department of Earth and Atmospheric Sciences, University of Houston, 312 Science & Research Building 1, Houston, TX 77204, USA
[2]National Institute of Environmental Research, Incheon, Republic of Korea
[3]Division of Environmental Engineering, Ajou University, Suwon, Republic of Korea
[4]Department of Atmosphere Sciences, Yonsei University, Seoul, Republic of Korea

Correspondence to: Yunsoo Choi (ychoi6@uh.edu)

Received: 10 July 2016 – Published in Geosci. Model Dev. Discuss.: 21 July 2016
Revised: 20 September 2016 – Accepted: 26 September 2016 – Published: 17 October 2016

Abstract. This study suggests a new modeling framework using a hybrid Eulerian–Lagrangian-based modeling tool (the Screening Trajectory Ozone Prediction System, STOPS) for a prediction of an Asian dust event in Korea. The new version of STOPS (v1.5) has been implemented into the Community Multi-scale Air Quality (CMAQ) model version 5.0.2. The STOPS modeling system is a moving nest (Lagrangian approach) between the source and the receptor inside the host Eulerian CMAQ model. The proposed model generates simulation results that are relatively consistent with those of CMAQ but within a comparatively shorter computational time period. We find that standard CMAQ generally underestimates PM_{10} concentrations during the simulation period (February 2015) and fails to capture PM_{10} peaks during Asian dust events (22–24 February 2015). The underestimation in PM_{10} concentration is very likely due to missing dust emissions in CMAQ rather than incorrectly simulated meteorology, as the model meteorology agrees well with the observations. To improve the underestimated PM_{10} results from CMAQ, we used the STOPS model with constrained PM concentrations based on aerosol optical depth (AOD) data from the Geostationary Ocean Color Imager (GOCI), reflecting real-time initial and boundary conditions of dust particles near the Korean Peninsula. The simulated PM_{10} from the STOPS simulations were improved significantly and closely matched the surface observations. With additional verification of the capabilities of the methodology on emission estimations and more STOPS simulations for various time periods, the STOPS model could prove to be a useful tool not just for the predictions of Asian dust but also for other unexpected events such as wildfires and oil spills.

1 Introduction

Particulate matter (PM) is one of the key air pollutants in the lower atmosphere. Numerous studies have reported its adverse effects on human health and the environment (Park et al., 2005; Heo et al., 2009; Jeon et al., 2015). Extreme levels of PM and the frequent occurrence of high PM events in the east Asia region have become a major social issue, particularly in South Korea (Korea, hereafter). This is because the region is geographically downwind from China and several desert areas, which are the source of significant emissions. Dust emissions from Mongolia and the Gobi Desert (Chun et al., 2001; Kim et al., 2008; Heo et al., 2009) cause extraordinarily severe yellow sand storms that often cover the entire sky over Korea during the spring and late winter. These result in reduced visibility (Chun et al., 2001) and increased mortality due to cardiovascular and respiratory diseases (Kwon et al., 2002), and their adverse effects are more evident in

cities closer to source regions of the Asian dust (Kashima et al., 2016).

In response to the problems resulting from Asian dust, the Ministry of Environment of Korea has undertaken $PM_{2.5}$ and PM_{10} forecasting since 2015 to prevent possible harm caused by high PM concentrations. However, the forecasts sometimes fail to capture high-level PM events. Accurate PM forecasting is challenging because of the complicated physical and chemical properties of PM and uncertainties in meteorology and emissions (Gelencser et al., 2007; Kim et al., 2008; Tie et al., 2009).

A number of modeling studies have shown the important role of meteorology in PM (Pai et al., 2000; Otte, 2008a, b), and some have suggested a variety of optimization techniques for enhancing the accuracy of meteorology (Ngan et al., 2012; S.-H. Lee et al., 2011; Choi et al., 2012; Jeon et al., 2014, 2015; Li et al., 2016). Additionally, accurate and updated emission inventories are essential to more accurate PM forecasting. Several studies have used anthropogenic emissions inventories for the Asia domain, such as the International Chemical Transport Experiment – Phase B (INTEX-B) emissions inventory in 2006 and a mosaic Asian anthropogenic emissions inventory in 2010 (MIX) for reliable model performance (Zhang et al., 2009; Zhao et al., 2012; Li et al., 2015). However, the use of the optimized meteorology and the most recent emissions inventory as input data for PM simulations can provide accurate forecasting results for only "normal" time periods, not "upset" events such as Asian dust. This problem is further exacerbated because of the high uncertainty in dust emissions.

To address this issue, the intent of this study is to introduce a modeling tool for PM simulation that can be used in conjunction with the Community Multi-scale Air Quality (CMAQ) model (Byun and Schere, 2006) to more accurately predict PM concentrations, using an Asian dust storm event as a case study. We apply a hybrid Eulerian–Lagrangian model, the Screening Trajectory Ozone Prediction System (STOPS), to simulate PM in the east Asia region. The model setup includes a moving nest domain between the source and the receptor inside the host CMAQ structure. STOPS provides simulation results similar to those of CMAQ, but does it so much faster than the full CMAQ modeling system. Additional details of the original version of STOPS (v1.0) and its effectiveness for regional air quality simulations are explained by Czader et al. (2015). However, since STOPS v1.0 was based on CMAQ v4.4, it is incompatible for recent PM simulations due to outdated modules and chemical mechanisms. Hence, we have implemented a new version of STOPS (v1.5) into CMAQ v5.0.2, which can be utilized with recent emissions inventories, improved chemical mechanisms and useful analyzing tools for the better simulation of Asian dust events.

The primary purpose of this study is to characterize underestimated PM concentrations by standard CMAQ and to determine the primary reason why CMAQ does not accurately capture PM peaks during the Asian dust events. We introduce a new modeling framework using STOPS as an alternative to full CMAQ modeling for the prediction of severe dust storms over the Korean Peninsula. We utilize STOPS for PM modeling and constrain PM concentrations using real-time satellite data from the Geostationary Ocean Color Imager (GOCI) sensor that allow STOPS to take into account the mostly updated input data (e.g., initial and boundary conditions and emission estimates) inside the modeling domain. We conduct several STOPS simulations using constrained PM concentrations and compare the results to corresponding surface observations to investigate whether the constrained PM concentrations produce accurate PM simulations. We ultimately conclude by proposing the STOPS forecasting/modeling system as an effective tool for capturing severe dust events over east Asia, particularly in Korea.

2 Methodology

2.1 STOPS

STOPS is a hybrid Eulerian–Lagrangian-based modeling tool derived from the CMAQ model. As shown in Fig. 1, a small subdomain of STOPS was configured inside the CMAQ domain and it moves along with the mean wind from CMAQ. Since STOPS inherits meteorological fields and initial and boundary conditions from a "host" CMAQ simulation, the movement of the STOPS domain is limited to the domain of the host CMAQ simulation. STOPS has the same vertical structure and simulates the same physical and chemical processes as CMAQ, except for the calculation of advection fluxes. CMAQ uses horizontal wind velocity (u and v) from WRF to calculate horizontal advection fluxes, but STOPS calculates the difference between a cell horizontal wind velocity and the mean horizontal velocity in STOPS domain (Czader et al., 2015), so it can consider the moving speed and direction of STOPS domain for the calculation of advection fluxes. Since the STOPS domain moves over time, the horizontal velocity from WRF should be adjusted based on the movement of the STOPS domain. The movement of the STOPS domain is determined by the layer-averaged horizontal wind in the center column from the bottom layer up to the top of planetary boundary layer (PBL), weighted by the layer thickness. The averages of the u and v components are calculated by the following equations (Eqs. 1–2):

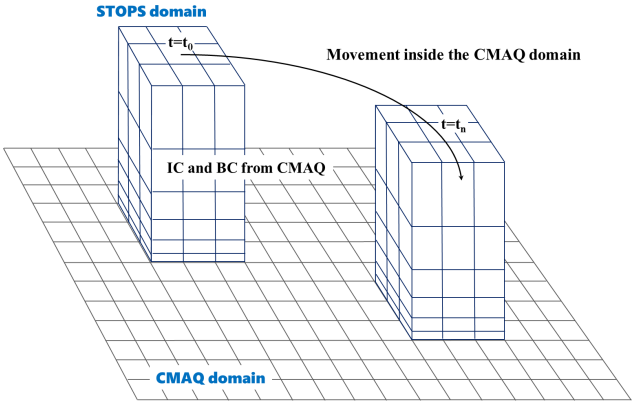

Figure 1. Conceptual diagram showing the basic structure and movement of the STOPS domain inside the CMAQ domain.

$$\bar{u} = \frac{1}{\sum_{L=1}^{\mathrm{PBLH}} \Delta\sigma_F(L)} \sum_{L=1}^{\mathrm{PBLH}} u_L \cdot \Delta\sigma_F(L) \quad (1)$$

$$\bar{v} = \frac{1}{\sum_{L=1}^{\mathrm{PBLH}} \Delta\sigma_F(L)} \sum_{L=1}^{\mathrm{PBLH}} v_L \cdot \Delta\sigma_F(L), \quad (2)$$

where $\sigma_F = 1 - \sigma$ and σ is the scaled air pressure in a sigma coordinate system (dimensionless) defined as

$$\sigma = \frac{(p - p_\mathrm{t})}{(p_\mathrm{s} - p_\mathrm{t})}, \quad (3)$$

where p, p_t, and p_s denote air pressure at the current level and the top and surface levels of the model, respectively. Czader et al. (2015) present more details on the model and its applications. The first version of STOPS (v1.0) was based on CMAQ v4.4 (Czader et al., 2015), but in this study, it has been updated to v1.5, and implemented in CMAQ v5.0.2.

2.2 Modeling system

In this study, we configured the CMAQ (v5.0.2) model domain with a grid resolution of 27 km (174 × 128) covering the northeastern part of Asia (Fig. 2) and 27 vertical layers extending from the surface to 100 hPa. This CMAQ domain, which is slightly larger than standard domain for east Asia study suggested by the Clean Air Policy Modeling System (CAPMOS) (http://capmos.nier.go.kr/guideline/guide_line.pdf) of the National Institute of Environmental Research (NIER) in Korea, covers more areas of the Gobi Desert, which is a major source of Asian dust.

Anthropogenic emissions for the CMAQ domain were obtained from the MIX emission inventory in 2010 (Li et al., 2015). This inventory contains gridded (0.25° × 0.25°) emission information for black carbon (BC), carbon monoxide (CO), carbon dioxide (CO_2), nitrogen oxides (NO_x), ammonia (NH_3), organic carbon (OC), fine and coarse particulate matter ($PM_{2.5}$ and PM_{10}), sulfur dioxide (SO_2), and non-methane volatile organic compounds (NMVOCs). To acquire high-resolution (1 km × 1 km) anthropogenic emissions in Korea, this study also used the Clean Air Policy Support System (CAPSS) emissions inventory in 2011 from NIER (D. G. Lee et al., 2011). The CAPSS inventory contains area, line, and point sources of CO, NH_3, NO_x, sulfur oxides (SO_x), total suspended particles (TSPs), PM_{10}, and VOCs. The emissions for the CMAQ simulations were prepared by the Sparse Matrix Operator Kernel Emissions (SMOKE) model (Houyoux et al., 2000). The carbon bond chemical mechanism (CB05) (Yarwood et al., 2005) and the AERO6 aerosol module (Nolte et al., 2015) were used for gas-phase and aerosol chemical mechanisms, respectively. The initial and boundary conditions were obtained from the standard CMAQ profile.

We simulated meteorological fields using the Weather Research and Forecast (WRF, v3.7) model (Skamarock et al., 2008) and used the 1° × 1° Final Operational Global Analysis (FNL) data of the National Centers for Environmental Prediction (NCEP) to determine the initial and boundary conditions. To improve the accuracy of meteorological fields, we adopted the optimized grid analysis nudging options suggested by Jeon et al. (2015) for the east Asia simulations.

The WRF-CMAQ simulations were conducted for the period of 21 January to 28 February in 2015, which included the first 10 days for spin-up. Evaluations applied to the month of February and the 3-day Asian dust event which occurred during 22–24 February 2015 (Table 1). During the event days, massive plumes of dust over the Gobi Desert and Mongolia region were transported to the Korean Peninsula. This happened due to the southeastward wind resulting from high pressure over the Mongolia region and low pressure over the northeastern part of China (Fig. S1 in the Supplement). The detailed options used for WRF and CMAQ simulations are listed in Tables S1 and S2 in the Supplement.

The configuration of the CMAQ subdomain for the STOPS simulation consists of 61 × 61 horizontal grid cells that cover a portion of the Korean Peninsula and the Yellow Sea. The initial position was near the northern part of the Yellow Sea (40° N, 121° E) (Fig. 2), which was the primary transport pathway of Asian dust. The simulated PM_{10} concentrations of the standard STOPS during Asian dust events (22–24 February 2015) closely agreed with those of CMAQ (Fig. S2 in the Supplement). The correlation coefficients (R) for each day were 0.94, 0.96, and 0.97, indicating that the results from STOPS and CMAQ are significantly correlated. This reasonable consistency of STOPS and CMAQ results justifies the use of STOPS instead of CMAQ in this study.

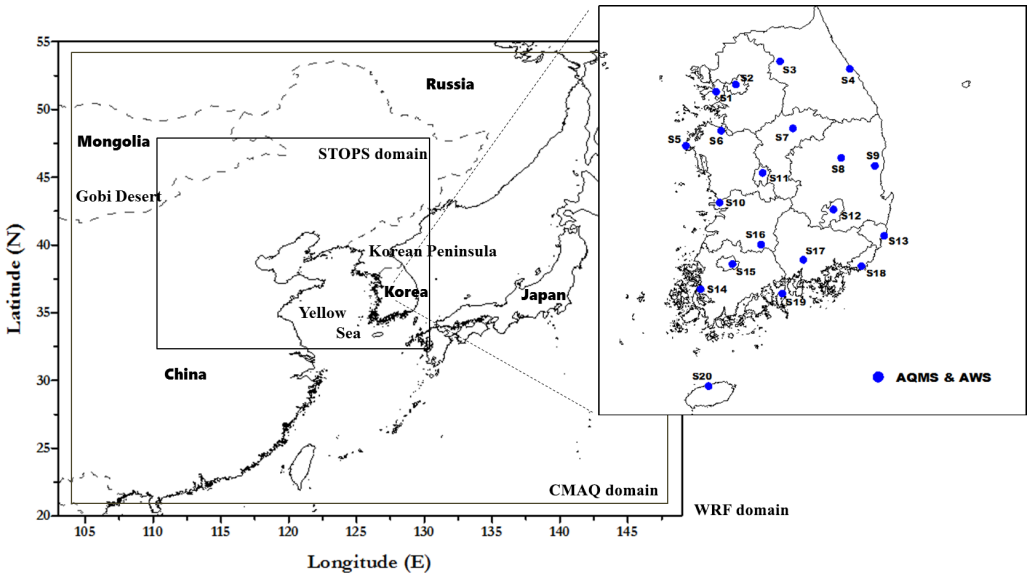

Figure 2. Domains for the WRF, CMAQ, and STOPS modeling. The right panel shows the location of the air quality monitoring stations (AQMS) and automatic weather system (AWS) sites used in this study.

Table 1. Observed PM_{10} and $PM_{2.5}$ concentrations ($\mu g\,m^{-3}$) recorded on each day of an Asian dust event in February 2015. The values are averaged of the 20 AQMS sites shown in Fig. 2. D_Max denotes daily maximum concentrations and D_Mean daily mean concentrations.

	PM_{10}		$PM_{2.5}$	
	D_Max	D_Mean	D_Max	D_Mean
22 Feb	345.47	111.52	28.75	18.85
23 Feb	472.47	341.63	72.67	43.61
24 Feb	175.88	111.86	37.78	23.46

2.3 In situ and satellite measurements

This study used surface observational data from the Air Quality Monitoring Station (AQMS) network operated by NIER. The network measures real-time air pollutant concentrations and provides hourly concentrations for CO, NO_2, O_3, $PM_{2.5}$, PM_{10}, and SO_2. We gathered the measured $PM_{2.5}$ and PM_{10} data in 2015 from the AQMS network, and the meteorological data were obtained from the Automatic Weather System (AWS) network operated by the Korea Meteorological Administration (KMA). The following statistical parameters were used for the evaluation of the performance of WRF and CMAQ simulations: index of agreement (IOA), mean bias error (MBE), and root mean square error (RMSE). These are defined as

$$\mathrm{IOA} = 1 - \frac{\sum_{i=1}^{N}(P_i - O_i)^2}{\sum_{i=1}^{N}\left(\left|P_i - \bar{O}\right| + \left|O_i - \bar{O}\right|\right)^2}$$

$$\mathrm{MBE} = \frac{\sum_{i=1}^{N}(P_i - O_i)}{N}$$

$$\mathrm{RMSE} = \sqrt{\frac{\sum_{i=1}^{N}(P_i - O_i)^2}{N}},$$

where N is number of data points and P_i and O_i denote CMAQ-simulated and observed concentrations, respectively.

We also employed the aerosol optical depth (AOD), measured by a GOCI sensor from the geostationary orbit onboard the Communication Ocean and Meteorological Satellite (COMS). The GOCI level 1B (L1B) data provide hourly daylight spectral images (09:30–16:30 LST, 8 times a day) for east Asia. The spatial coverage extends to 2500 km × 2500 km centered at 36° N, 130° E (Lee et al., 2010; Choi et al., 2016). The AOD at 550 nm with a 6 km resolution were obtained from GOCI L1B data using a retrieval algorithm introduced by Choi et al. (2016). The GOCI-derived AOD data were used for constraining of PM concentrations and the model evaluation. For the evaluation of CMAQ-simulated PM_{10}, we converted the concentration units in CMAQ to AOD for a fair comparison of the results with GOCI. The aerosol properties from the CMAQ simulation (CMAQ-derived AOD) were obtained by the following equations (Eqs. 4–6), which were introduced by Roy et al. (2007) and have successfully been tested in east Asia

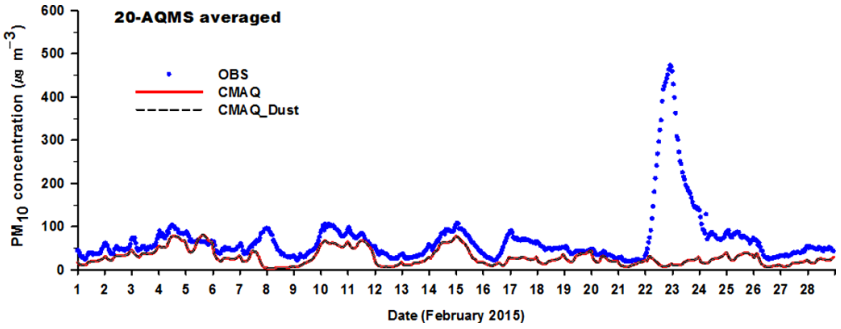

Figure 3. Time series of observed (OBS: blue dots) and simulated (CMAQ: red line, CMAQ_Dust: black dashed line) PM_{10} concentrations in February 2015. The values are averaged values for 20 AQMS sites: CMAQ_Dust is closely coupled with the standard CMAQ modeling results (red line).

(Song et al., 2008; Park et al., 2011):

$$\mathrm{AOD_{CMAQ}} = \sum_{i=1}^{N} (\sigma_{\mathrm{sp}} + \sigma_{\mathrm{ap}})_i \, \Delta Z_i \tag{4}$$

$$\sigma_{\mathrm{sp}} = (0.003)\, f_t\,(\mathrm{RH}) \left[\mathrm{NH_4^+} + \mathrm{SO_4^-} + \mathrm{NO_3^-}\right] + (0.004)\,[\mathrm{OM}] + (0.001)\,[\mathrm{FS}] + (0.0006)[\mathrm{CM}] \tag{5}$$

$$\sigma_{\mathrm{ap}} = (0.01)\,[\mathrm{LAC}], \tag{6}$$

where i is the vertical layer number, ΔZ is the layer thickness, and the brackets indicate mass concentrations in $\mathrm{mg\,m^{-3}}$ units. The OM, FS, CM, and LAC denote mass concentrations of organic species, fine soil, coarse particles, and light-absorbing carbon, respectively. The specific scattering coefficients in the equations (i.e., 0.003, 0.004, 0.001, 0.0006, and 0.001) are represented in units of $\mathrm{m^2\,mg^{-1}}$. The $f_t\,(\mathrm{RH})$, calculated by the method described by Song et al. (2008), denotes relative humidity based on the aerosol growth factor.

3 PM_{10} simulation results from standard CMAQ

3.1 Comparison with surface measurement

We simulated PM_{10} concentrations by standard CMAQ and compared them with surface observational data obtained from the AQMS network of NIER in Korea. For this comparison, we selected 20 AQMS sites, evenly distributed in Korea (Fig. 2), and calculated mean PM_{10} concentrations at all of the sites. We do not present the results for $PM_{2.5}$ because the simulated $PM_{2.5}$ exhibited almost the same temporal variation and lower concentrations to those of PM_{10}. In addition, the coarse particles comprise a major portion of the total PM during the Asian dust period, as described by Chun et al. (2001). From the comparison shown in Fig. 3, the concentration of CMAQ-simulated PM_{10} was slightly underestimated, but its temporal variation showed reasonably close agreement with observations except for the Asian dust episode (22–24 February 2015). The CMAQ failed to capture the high peaks of PM_{10} in the episode caused by the transport of the massive dust from the Gobi Desert and Mongolia region.

As shown in Table 2, the performance of CMAQ simulation for the entire period (February 2015) was poor. For example, the high value of RMSE ($78.03\,\mu\mathrm{g\,m^{-3}}$), low value of IOA (0.36), and negative value of MBE ($-39.94\,\mathrm{mug\,m^{-3}}$) indicate that CMAQ underestimated PM_{10} and its temporal variation did not agree well with the observations. The calculated statistics for the period excluding the Asian dust episodes was much better than those for the entire period, as indicated in Table 2. The large differences in these findings clearly reveal that the performance of CMAQ is relatively accurate for the regular simulation period, but it is not for the Asian dust period. As shown in Fig. 4 and Table S3, meteorological fields such as temperature and wind speed in the receptor regions (Korea) showed close agreement with observations, even during the Asian dust period. It suggests that the underestimated PM_{10} concentrations were likely due to the uncertainty in meteorology in the source regions (China and Mongolia) and/or faulty estimation of dust emissions for the CMAQ simulation. We attributed the main reason for the PM_{10} underestimation to poorly estimated dust emission because CMAQ showed poor performance only during the Asian dust period.

To enhance the performance of CMAQ for PM_{10} simulations during the Asian dust period, we employed the in-line windblown dust module in CMAQ v5.0.2. The module calculates the vertical dust emission flux (F) by following formula described by Fu et al. (2014):

$$F = \sum_{i=1}^{M}\sum_{j=1}^{N} K \times A \times \frac{\rho}{g} \times S_i \times \mathrm{SEP} \times u_* \times (u_*^2 - u_{*ti,j}^2), \tag{7}$$

where i and j represent the type of erodible land and soil, K is the ratio between vertical and horizontal flux, A is the particle supply limitation, ρ is the air density, g is the gravitational constant, S_i is the area of the dust source, SEP is the

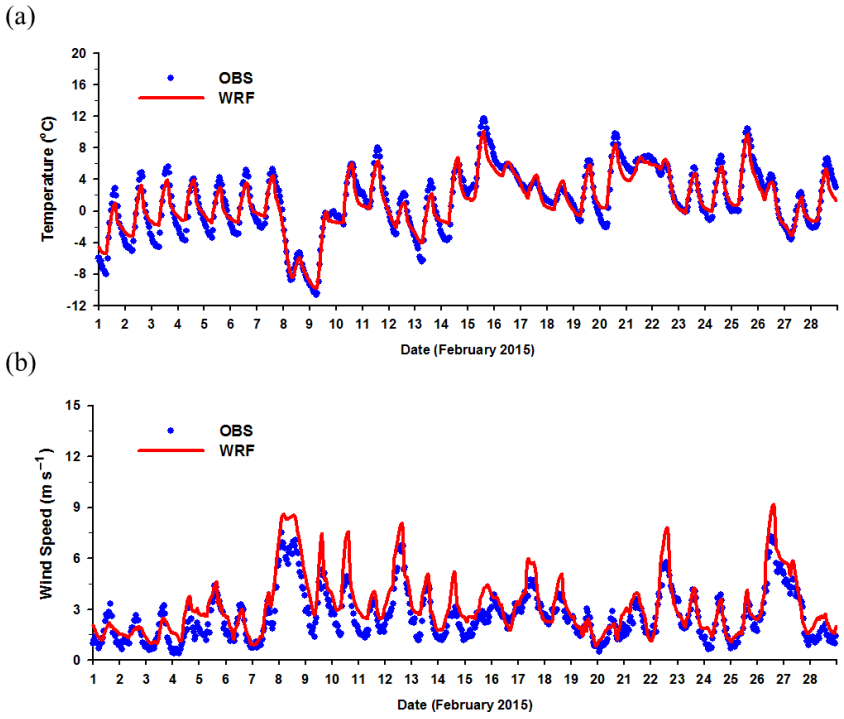

Figure 4. Time series of observed (OBS: blue dots) and WRF-simulated (WRF: red line) **(a)** temperature and **(b)** wind speed in February 2015. The values are averaged values for 20 AQMS sites.

Table 2. Statistical parameters of PM_{10} concentrations at 20 AQMS sites in Korea for the simulations without the dust module (CMAQ), with the in-line dust module (CMAQ_Dust).

	Entire period			Without dust events		
	RMSE	IOA	MBE	RMSE	IOA	MBE
CMAQ	78.03	0.36	−39.94	28.56	0.81	−22.83
CMAQ_Dust	78.03	0.36	−39.94	28.56	0.81	−22.83

soil erodible potential, u_* is the friction velocity, and $u_{*ti,j}$ denotes the threshold friction velocity.

Interestingly, the employment of the in-line windblown dust module in CMAQ simulations did not provide discernible enhancement in PM_{10} concentrations (Table 2) because of lower friction velocity than the threshold in the module during the simulation period (February 2015) (Table S4 in the Supplement). Several studies have reported that the threshold friction velocity plays a key role in the calculation of dust emission flux because the threshold can determine the probability of the lifting of dust particles (Choi and Fernando, 2008; Fu et al., 2014). This research also implies that more studies that enhance the capability of dust modules during the winter period should be performed.

3.2 Comparison with satellite-based observation

Figure 5 presents a comparison of time-averaged AOD derived from GOCI and CMAQ. For an unbiased comparison of AOD, we removed grid cells from GOCI data consisting of fewer than 15 pixels (i.e., bad pixels) because of cloud contamination; we also did not include the corresponding grid cells in CMAQ for our comparison. The GOCI-derived AOD shows several blank areas in the northern part of the Korean Peninsula, near the northeastern region of China, and in most regions of Japan because of the significantly high fraction of clouds over these areas. The horizontal features of the CMAQ-derived AOD were similar to those of the GOCI-derived AOD, but CMAQ overestimated the AOD near the southeastern part of China. On the other hand, compared to the GOCI-derived AOD, the CMAQ underestimated the AOD over the Yellow Sea and Korea. As mentioned in Sect. 3.1, CMAQ underestimated surface PM_{10} concentrations in Korea. The CMAQ-derived AOD in Korea was also

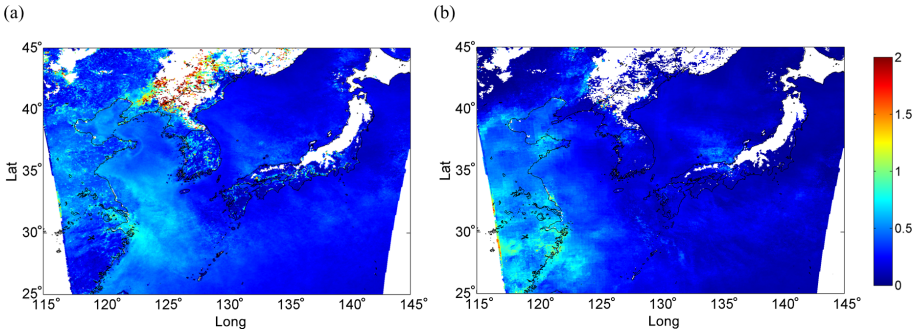

Figure 5. The **(a)** GOCI- and **(b)** CMAQ-derived AOD (550 nm) during the entire time period of simulations. The values are averaged for February 2015.

underestimated compared to GOCI-derived AOD, consistent with the surface measurements. These comparisons using the satellite and surface measurements indicated that the CMAQ was unable to capture the high levels of PM in Korea during the simulation period in this study (February 2015). Hence, the discrepancy between CMAQ- and GOCI-derived AOD is likely due to uncertainty in emissions of PM precursors such SO_2, NO_x, and NH_3 (Jeon et al., 2015) and meteorology over source regions as discussed in Sect. 3.1.

Compared to the GOCI-derived AOD, the CMAQ-derived AOD near the northern regions of the Korean Peninsula was underestimated. This underestimation may have resulted from the failure of CMAQ to simulate the Asian dust emissions and their transport to the Korean Peninsula on 22–24 February 2015. The CMAQ-derived AOD was underestimated primarily in the moving pathway of the Asian dust (i.e., between the Gobi Desert (source area) and the Korean Peninsula (receptor area)). As addressed in Sect. 3.1, the inline windblown dust module in CMAQ failed to accurately estimate the dust emissions during the Asian dust period and it caused the model to underestimate AOD near the northern regions of the Korean Peninsula.

To further investigate the issue of underestimation of CMAQ during the period of Asian dust (22–24 February 2015), we compared the GOCI- and CMAQ-derived AODs on each event day. Unfortunately, the comparison was available only on 22 February since the GOCI-derived AOD included a significantly high number of blank pixels on the other event days because of the high fraction of cloud cover. Figure 6 shows GOCI- and CMAQ-derived daily mean (09:30–16:30 LST) AODs on 22 February. The GOCI-derived AOD clearly showed massive amounts of dust near the northwestern regions of the Korean Peninsula and the eastern part of China and densely distributed dust particles over the Yellow Sea that were transported from the Gobi Desert. In contrast, CMAQ did not reproduce the high dust concentrations near the Korean Peninsula because of the failure in the estimation of dust emissions.

We concluded that CMAQ clearly underestimated PM_{10} concentrations during the simulation period and failed to capture peaks during the Asian dust period starting on 22 February. Thus, we attempted to use STOPS for capturing the dust enhanced PM_{10} in Korea (receptor region). We used the dust storm data temporarily detected by satellite measurements between the source and receptor regions as an input for the STOPS modeling. The following sections describe the details of how STOPS was used for PM_{10} forecasting.

4 Application of STOPS for PM_{10} forecasting

Assuming the CMAQ PM_{10} simulation results in this study were used for forecasting purposes, the severe dust events starting on 22 February 2015 could not be predicted. Thus, to accurately forecast the transport of the massive dust storm, we must take into account the most recent and accurate initial and boundary conditions and emissions. Figure 7 shows the GOCI-derived AOD on 21–22 February, when a dust storm was approaching Korea (receptor region). The massive dust storm was not evident from the GOCI-derived AOD on 21 February, but a center of the dust storm in the northwestern region of the Korean Peninsula was first seen at 10:30 LST on 22 February. Upon observation of the massive dust concentrations from the GOCI-derived AOD at 10:30 LST on 22 February, a new PM_{10} forecasting using STOPS with real-time AOD data can be performed in a short time (i.e., a few minutes). The current forecasting results can then be replaced by the results from the STOPS. For the new PM_{10} forecasting using STOPS, we intended to use the GOCI-derived AOD as a new initial condition for PM_{10} species. However, the approach does not fully consider continuous transport of dust from the source regions because the impact of the changed initial condition on the STOPS results would be diminished within a few hours. Thus, we used the GOCI-derived AOD as PM emissions for the STOPS forecasting to make the best use of the AOD data.

4.1 Satellite-adjusted PM concentrations

For the new PM_{10} forecasting using STOPS, we first attempted to convert the GOCI-derived AOD to PM concentra-

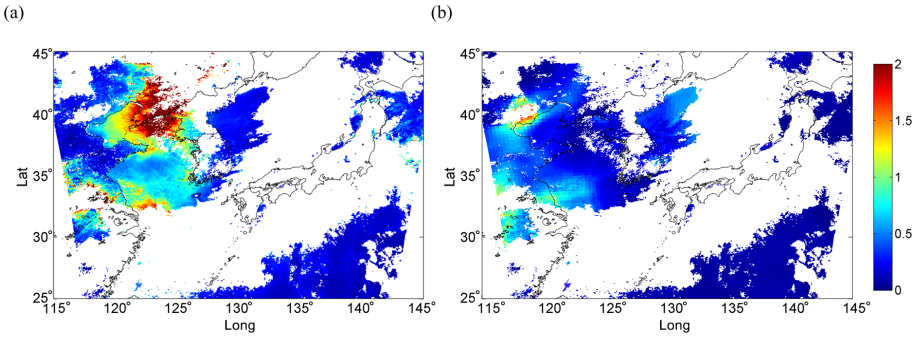

Figure 6. The **(a)** GOCI- and **(b)** CMAQ-derived AODs (550 nm) on 22 February 2015. The values are averaged from 09:30 to 16:30 LST.

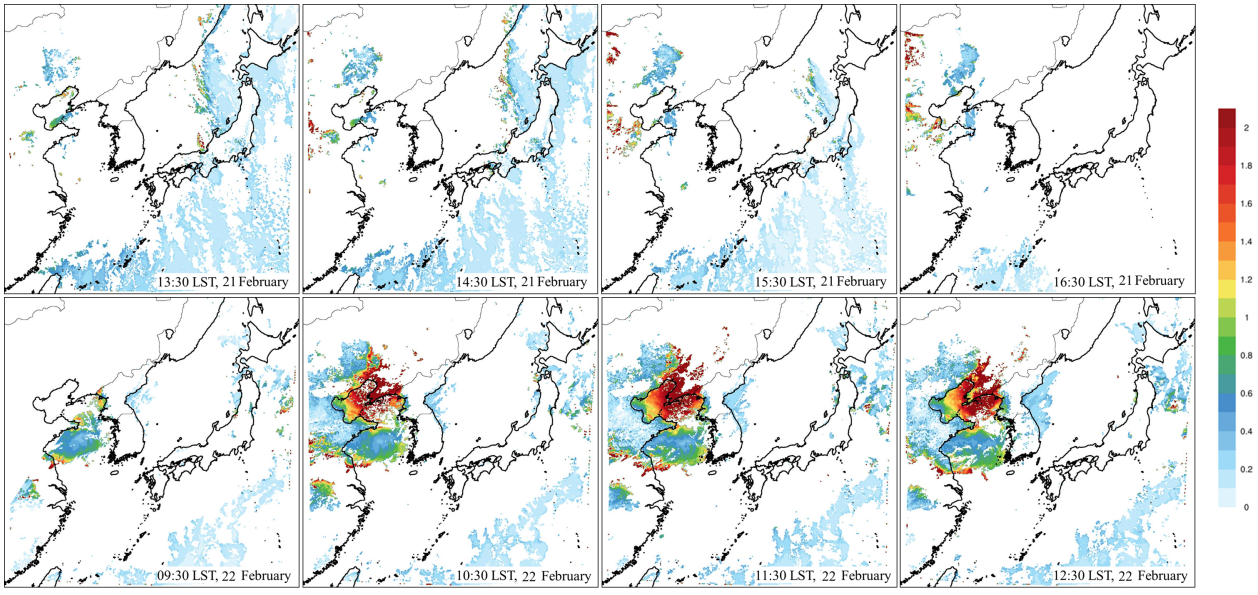

Figure 7. The GOCI-derived AOD (550 nm) from 13:30 LST on 21 February to 12:30 LST on 22 February 2015. The white-colored areas represent missing pixels.

tions and directly add them to the simulated PM concentrations by STOPS. However, the sudden and rapid changes in PM concentration made the STOPS simulation unstable and they sometimes caused unexpected termination of STOPS runs due to overflow error. To resolve this problem, we regarded the GOCI-derived AOD as PM emissions and indirectly constrained the original PM concentrations by using the alternative emissions. In short, the GOCI-derived AOD was converted to emissions and used for the STOPS forecasting. We should note that the alternative emissions are not real, but are rather the enhanced dust concentrations which are taking the form of emissions. We concluded this methodology could be an effective way to reflect the satellite-measured AOD to STOPS simulation without possible computational error.

As indicated in Fig. 7, the massive dust storm was first captured by the GOCI-derived AOD at 10:30 LST on 22 February 2015, so we adjusted the standard emissions at a corresponding time based on the GOCI-derived AOD and used them for the STOPS forecasting. We should note that the AOD and the emission rate are expressed in different units; the AOD is a unitless value, while the emission rate is expressed in units of grams per second (particles) or moles per second (gas-phase species); therefore, we employed a scaling factor to convert the AOD to the emission rate. To find a reasonable scaling factor, we regridded the domain of the GOCI-derived AOD data so that they corresponded with the CMAQ domain and compared the AOD in each grid cell with corresponding emission rates of total PM in the MIX inventory (e.g., PM_{10}). We used only the grid cells with valid AODs (no missing values) and emission rate (> 0) for the comparison and then calculated the average ratio of the AOD to emission rates. The calculated ratio was 1884.49 g s^{-1} for this case, indicating that the emission rate of total PM inside the modeling domain was 1884.49 times larger than the GOCI-derived AOD. It should be noted that the ratio cannot generally ex-

plain the relationship between AOD and emissions. Because the relationship is valid for only a particular domain (Fig. 2) and time (10:30 LST on 22 February 2015), the ratio for each case should be recalculated.

For the unit conversion from AOD to the emissions rate of total PM, we used the estimated ratio as a scaling factor and calculated the total PM emissions by the following equation (Eq. 8):

$$\mathrm{PMT}_{i,j} = \mathrm{AOD}_{i,j} \times \mathrm{SF}, \quad (8)$$

where $\mathrm{PMT}_{i,j}$ and $\mathrm{AOD}_{i,j}$ represent the emission rates of total PM and GOCI-derived AOD in each grid cell, respectively. SF is the calculated scaling factor ($1884.49\,\mathrm{g\,s^{-1}}$), which indicates the relationship between the AOD and the emission rate.

For the STOPS simulation, we split the calculated $\mathrm{PMT}_{i,j}$ into several specific species, including coarse and fine particles, used for the CB05–AERO6 chemical mechanism. In order to calculate the species distribution, we estimated the mass fractions of each PM species during the Asian dust events based on the findings in Kim et al. (2005) and Stone et al. (2011), which described the composition of measured PM during the Asian dust periods (Table 3). More than half of the $\mathrm{PMT}_{i,j}$ was allocated to coarse particles (PMC) because they comprise a major percentage of Asian dust, as reported in several studies (Kim et al., 2003; Kim et al., 2005; Lee et al., 2004; Stone et al., 2011). The speciated PM emissions were injected into standard PM emissions in each grid cell. Based on the findings by Kim et al. (2010), the amounts of the alternative emissions were assumed to be distributed below the altitude of 3 km (1 to 11 vertical layers). The entire procedures of the new PM forecasting by STOPS using GOCI-derived AOD are briefly depicted in Fig. S3.

4.2 Enhanced PM_{10} forecasting using STOPS

We conducted a new PM_{10} forecasting run using STOPS with the constrained PM concentrations (by using alternative emissions) and examined the improvement in its accuracy over that of the standard CMAQ model. The STOPS forecasting covers 1 day (24 h), which began at 11:00 LST on 22 February 2015, immediately following the massive dust were first observed in the GOCI-derived AOD between the source and receptor regions.

Figure 8 shows the comparison of the PM_{10} concentration from CMAQ using standard emissions and STOPS using alternative emissions. The PM_{10} from standard CMAQ exhibited high concentrations over the eastern part of China, central Yellow Sea, and northwestern part of the Korean Peninsula. By contrast, the constrained PM_{10} by the alternative emissions (Fig. S4 in the Supplement) exhibited significantly increased concentrations, particularly in the northwestern part of the Korean Peninsula (Fig. 8). The constrained PM_{10} concentration showed similar features as those of the GOCI-derived AOD, shown in Fig. 6a, implying that the dense dust attributed by Asian dust was accurately reflected in the STOPS forecasting.

We should note that the duration of the release of alternative emissions strongly affected the simulated PM_{10}. Hence, it plays an important role in the STOPS forecasting, so we conducted four forecasting runs with different release durations (3, 6, 12, and 24 h) as shown in Fig. 9. The results from the four STOPS runs were then compared with those from standard CMAQ and available PM_{10} surface measurements. Figure 9 exhibits clear differences in the temporal variation of PM_{10} resulting from the impact of the release durations. As addressed in Sect. 3.1, the standard CMAQ run failed to capture the drastic increase in PM_{10} concentrations on 22 February 2015 because of the poor dust emission modeling in CMAQ. However, the STOPS forecasting showed significantly improved PM_{10} results compared to standard CMAQ. The results indicated higher PM_{10} concentrations than those of CMAQ, and they were much closer to observations.

Interestingly, Fig. 9 shows that predicted PM_{10} by STOPS with a duration of release of 3 h (STOPS_E3) closely agreed with observations during the first 3 h. However, the simulated PM_{10} began to decrease immediately after the third hour, and the agreement with observations gradually worsened with time. The results of the other STOPS runs with different durations of release of 6, 12, and 24 h (STOPS_E6, STOPS_E12 and STOPS_E24, respectively) were almost the same as those of STOPS_E3. In other words, the impact of the alternative emissions on the PM_{10} prediction highly depends on the durations of emission release and the impact was gone after the release ended. STOPS_E24 represented the closest agreement with observations, implying that STOPS_E24 produced the greatest improvement in 1-day PM_{10} forecasting because of continuous emissions during the entire forecasting time (24 h).

Despite its positive performance in 1-day PM_{10} forecasting, STOPS_E24 did not perfectly capture the high PM_{10} concentrations during the Asian dust event. In fact, it underestimated the peak of observed PM_{10}, which may have resulted from uncertainty inherent in the methodology using AOD estimation. Direct conversion from the AOD to the alternative emissions rate using a scaling factor is challenging because it has not yet been proven reliable by existing studies. Hence, the uncertainty inherent in unit conversion might have contributed to the inaccuracy of the emissions rate. In addition, the GOCI-derived AOD data contained missing data due to the cloud cover over the study area during the event on 22 February and, as a consequence, it did not accurately represent the distribution of transported Asian dust. The most probable reason for the underestimated PM_{10} simulated by STOPS was that the alternative emissions during the first time step (11:00 LST on 22 February 2015) were subsequently used for all of the time steps without accounting for spatiotemporal variations. Since the horizontal and vertical distributions of the Asian dust changed with time, the alter-

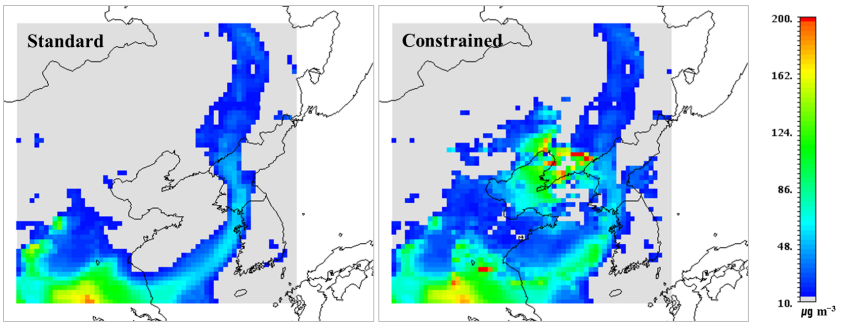

Figure 8. Difference of the simulated PM_{10} concentrations ($\mu g\,m^{-3}$) between the standard CMAQ run (left) and STOPS forecasting run with alternative emissions estimated according to GOCI-derived AOD (right) inside the STOPS domain at 12:00 LST on 22 February 2015.

Table 3. Specific fractions (%) for the splitting of total PM emission into specific PM species in the CB05–AERO6 chemical mechanism used in this study.

PM emission species	Fraction	PM emission species	Fraction
PMC (coarse particle)	55 %	PCA (calcium)	2 %
PMOTHR (unspeciated $PM_{2.5}$)	25 %	PEC (elemental carbon)	1 %
PSO_4 (sulfate)	8 %	PNA (sodium)	1 %
PNO_3 (nitrate)	3 %	PCL (chloride)	1 %
POC (organic carbon)	3 %	PK (potassium)	1 %
PNH4 (ammonium)	2 %		

native emissions in the first time step did not accurately represent the varied dust distribution in the next time step. The uncertainty with regard to the alternative emissions increases with time. The STOPS_E24-predicted PM_{10} concentrations showed close agreement with observations during the first 6 h (Fig. 9), but error gradually widened with time. However, as observation in later hours cannot be reflected at the beginning of forecasting, such a problem is inevitable in a forecasting mode. Thus, repeated forecasting for short time periods (e.g., 6 h) with the variable alternative emissions could possibly provide more accurate PM_{10} results for the Asian dust events. STOPS would be very useful for repeated PM_{10} forecasting because of its remarkably short simulation time (a few minutes).

To verify the horizontal distribution of PM_{10} resulting from the effect of constrained PM, we compared the simulated surface PM_{10} concentrations from the STOPS forecasting to those from standard CMAQ. Figure 10 shows the horizontal distribution of surface PM_{10} concentrations inside the STOPS domain simulated by standard CMAQ and STOPS_E24, which indicates the most accurate 1-day forecasting results of all the STOPS simulations (from Fig. 9). The location of the STOPS domain moved slightly toward the southeast according to the changed mean wind in the domain. In the first time step (0 h, 11:00 LST, 22 February), STOPS_E24 showed the same PM_{10} distribution as standard CMAQ because the initial condition for the STOPS simulation was provided by the standard CMAQ. After 8 h, the PM_{10} concentration from STOPS_E24 differed from that of the standard CMAQ due to the effect of the alternative emissions by the GOCI-derived AOD. After 16 and 24 h, the difference became more pronounced. Results of standard CMAQ did not show a high level of PM_{10}, but those of STOPS_E24 showed a PM_{10} concentration of at least $100\,\mu g\,m^{-3}$ near the Korean Peninsula. Specifically, they showed extremely high PM_{10} concentrations of over $1500\,\mu g\,m^{-3}$ in the northwestern part of the Korean Peninsula. Figure 7 (10:30 LST on 22 February) indicates massive dust over that area from the GOCI-derived AOD consistent with the enhanced PM_{10} concentrations. The massive dust over the region was transported to Korea and led to significantly enhanced levels of PM_{10}. The horizontal distributions of PM_{10} at higher vertical levels up to 3 km showed similar features at the surface layer because the alternative emissions were evenly distributed below that level.

Overall, even with the uncertainties addressed above, the massive dust storm near the Korean Peninsula on an Asian dust day was reasonably reproduced by the STOPS forecasting by using PM emissions constrained by GOCI-derived AOD. These results indicate that the STOPS could possibly be used for PM_{10} forecasting with real-time constraints of PM concentration and this methodology should enhance the performance of PM_{10} forecasting and modeling.

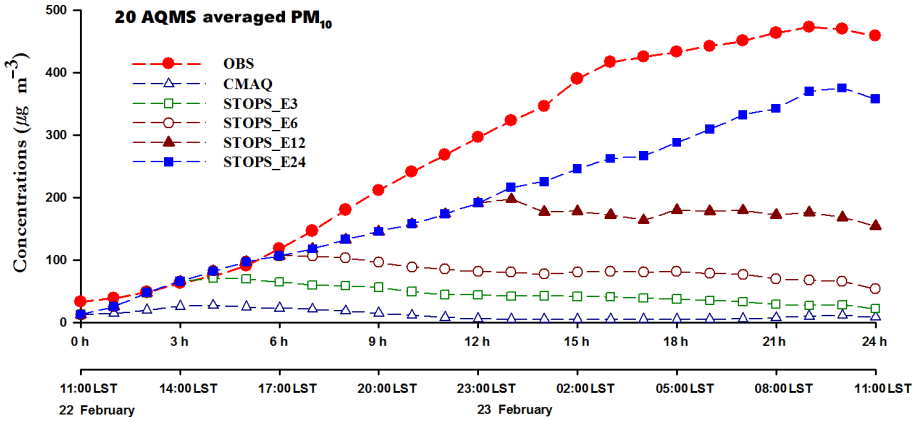

Figure 9. Comparison of observed, CMAQ-simulated, and STOPS-simulated PM_{10} concentrations during the 24 h from 10:00 LST on 22 February 2015.

5 Summary

This study introduced a revised modeling framework using a hybrid Eulerian–Lagrangian model (called STOPS) that showed almost the same performance as CMAQ, but used a shorter simulation runtime. STOPS v1.5 has been implemented into CMAQ v5.0.2 for PM_{10} simulations over the east Asia during Asian dust events and we investigated the possibility of using STOPS to enhance the accuracy of PM_{10} forecasting. During the entire simulation period (February 2015), the standard CMAQ underestimated PM_{10} concentrations compared to surface observations and failed to capture the PM_{10} peaks of Asian dust events (22–24 February 2015). With reasonable meteorological input, the underprediction of PM_{10} concentration was mainly due to the inaccurate estimation of dust emissions during this period used in CMAQ. We also evaluated the horizontal feature of CMAQ-simulated PM_{10} using satellite-observed data (GOCI). The PM_{10} results from the standard CMAQ run were compared to those of the GOCI-derived AOD and the results indicated that the standard CMAQ barely captured the transported dust from the Gobi Desert to the Korean Peninsula during the Asian dust events.

For more accurate PM_{10} prediction, we used the STOPS model and conducted several simulations using constrained PM concentrations (by using alternative emissions) based on the GOCI-derived AOD, which reflected the most recent initial and boundary conditions near the Korean Peninsula. The STOPS simulations showed higher PM_{10} concentrations than the standard CMAQ and indicated clear dependence on the duration of the alternative emission release. The STOPS simulations showed reasonable PM_{10} concentrations close to observational data, but they did not capture the peak during the Asian dust events because of uncertainty in the methodology used for the constraining PM concentrations. The direct conversion from AOD to emissions using a scaling factor was challenging because it has not yet been proven reliable by existing studies. In addition, the GOCI-derived AOD data were missing many values because of the high fraction of cloud cover during the event and consequently, it did not accurately reflect the massive dust storm on the Asian dust day.

Overall, STOPS reasonably reproduced the high level of PM_{10} over the Korean Peninsula during the Asian dust event with constrained PM concentrations using satellite measurements. Although STOPS indicated significantly high PM_{10} enhancement for the episode, it still requires improvement before its results can be generalized. Thus, we should direct our study toward additional verification of the methodology regarding unit conversion (e.g., possible nonlinearities) and numerous sensitivity simulations for different cases to determine the optimal duration of the release of the alternative emissions. The results of this study are an ideal starting point for such studies.

The ultimate goal of this study was to suggest an effective tool for successive PM_{10} forecasting and modeling over east Asia. The results clearly showed the reliability and various advantages of STOPS modeling. Therefore, because of its reliable performance with remarkably high computation efficiency, the STOPS model could prove to be a highly useful tool for enhancing dust forecasting/modeling performance over east Asia. Further, the benefit of STOPS modeling could be generalized to the forecasting and modeling of unexpected events such as wildfires and oil spills.

6 Code availability

The STOPS v1.5 source code can be obtained by contacting the corresponding author at ychoi6@uh.edu.

The Supplement related to this article is available online at doi:10.5194/gmd-9-3671-2016-supplement.

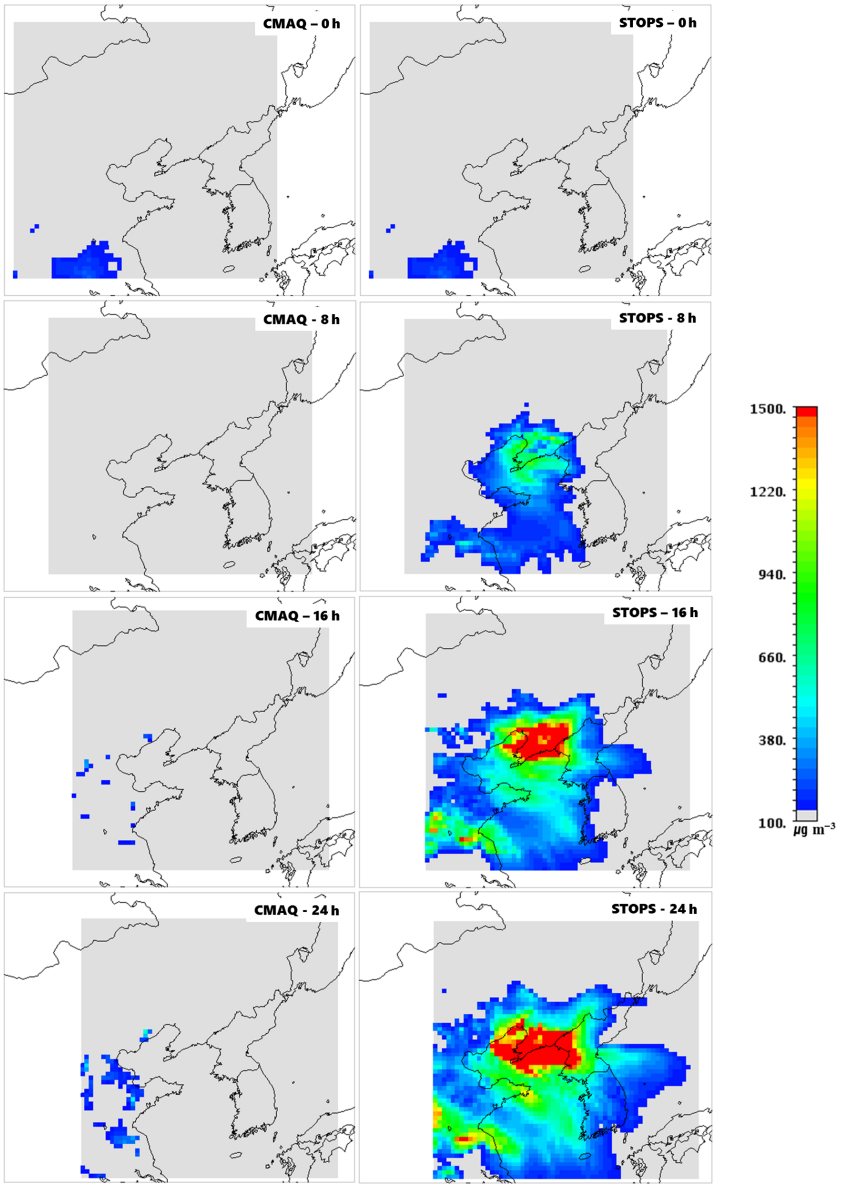

Figure 10. Horizontal distributions of standard CMAQ- and STOPS_E24-simulated surface PM_{10} concentrations inside the STOPS domain. The concentrations were recorded at 8 h intervals after the beginning of the simulation (11:00 LST on 22 February 2015).

Acknowledgements. This study was partially supported by funding from the Ministry of Environment of Korea (NIER-1900-1946-302-210). We thank the team members of GOCI and AQMS for the preparation of the remote sensing data and PM measurement data, respectively.

Edited by: A. B. Guenther
Reviewed by: two anonymous referees

References

Byun, D. and Schere, K. L.: Review of the governing equations, computational algorithms, and other components of the Models-3 Community Multiscale Air Quality (CMAQ) modeling system, Appl. Mech. Rev., 59, 51–77, doi:10.1115/1.2128636, 2006.

Choi, H.-J., Lee, H. W., Jeon, W.-B., and Lee, S.-H.: The numerical modeling the sensitivity of coastal wind and ozone concentration to different SST forcing, Atmos. Environ., 46, 554–567, doi:10.1016/j.atmosenv.2011.06.068, 2012.

Choi, M., Kim, J., Lee, J., Kim, M., Park, Y.-J., Jeong, U., Kim, W., Hong, H., Holben, B., Eck, T. F., Song, C. H., Lim, J.-H., and Song, C.-K.: GOCI Yonsei Aerosol Retrieval (YAER) algorithm and validation during the DRAGON-NE Asia 2012 campaign, Atmos. Meas. Tech., 9, 1377–1398, doi:10.5194/amt-9-1377-2016, 2016.

Choi, Y.-J. and Fernando, H. J. S.: Implementation of a windblown dust parameterization into MODELS-3/CMAQ: Application to

episodic PM events in the US/Mexico border, Atmos. Environ., 42, 6039–6046, doi:10.1016/j.atmosenv.2008.03.038, 2008.

Chun, Y., Boo, K.-O., Kim, J., Park, S.-U., and Lee, M.: Synopsis, transport, and physical characteristics of Asian dust in Korea, J. Geophys. Res., 106, 18461–18469, doi:10.1029/2001JD900184, 2001.

Czader, B. H., Percell, P., Byun, D., Kim, S., and Choi, Y.: Development and evaluation of the Screening Trajectory Ozone Prediction System (STOPS, version 1.0), Geosci. Model Dev., 8, 1383–1394, doi:10.5194/gmd-8-1383-2015, 2015.

Fu, X., Wang, S. X., Cheng, Z., Xing, J., Zhao, B., Wang, J. D., and Hao, J. M.: Source, transport and impacts of a heavy dust event in the Yangtze River Delta, China, in 2011, Atmos. Chem. Phys., 14, 1239–1254, doi:10.5194/acp-14-1239-2014, 2014.

Gelencser, A., May, B., Simpson, D., Sanchez-Ochoa, A., Kasper-Giebl, A., Puxbaum, H., Caseiro, A., Pio, C., and Legrand, M.: Source apportionment of $PM_{2.5}$ organic aerosol over Europe: Primary/secondary, natural/anthropogenic, and fossil/biogenic origin, J. Geophys. Res., 112, D23S04, doi:10.1029/2006JD008094, 2007.

Heo, J.-B., Hopke, P. K., and Yi, S.-M.: Source apportionment of $PM_{2.5}$ in Seoul, Korea, Atmos. Chem. Phys., 9, 4957–4971, doi:10.5194/acp-9-4957-2009, 2009.

Houyoux, M., Vukovich, J., and Brandmeyer, J.: Sparse Matrix Kernel EmissionsModeling System: SMOKE User Manual, MCNC-North Carolina Supercomputing Center, available at: http://www.cmascenter.org/ (last access: 12 October 2016), 2000.

Jeon, W.-B., Lee, S.-H., Lee, H., Park, C., Kim, D.-H., and Park, S.-Y.: A study on high ozone formation mechanism associated with change of NO_x / VOCs at a rural area in the Korean Peninsula, Atmos. Environ., 89, 10–21, doi:10.1016/j.atmosenv.2014.02.005, 2014.

Jeon, W., Choi, Y., Lee, H. W., Lee, S.-H., Yoo, J.-W., Park, J., and Lee, H.-J.: A quantitative analysis of grid nudging effect on each process of $PM_{2.5}$ production in the Korean Peninsula, Atmos. Environ., 122, 763–774, doi:10.1016/j.atmosenv.2015.10.050, 2015.

Kashima, S., Yorifujy, T., Bae, S., Honda, Yasushi, Lim, Y.-H., and Hong, Y.-C.: Asian dust effect on cause-specific mortality in five cities across South Korea and Japan, Atmos. Environ., 128, 20–27, doi:10.1016/j.atmosenv.2015.12.063, 2016.

Kim, H. M., Kay, J. K., and Jung, B.-J.: Application of Adjoint-based forecast sensitivities to Asian dust transport events in Korea, Water Air Soil Pollut., 195, 335–343, doi:10.1007/s11270-008-9750-8, 2008.

Kim, K.-H., Choi, G.-H., Kang, C.-H., Lee, J.-H., Kim, J. Y., Youn, Y. H., and Lee, S. R.: The chemical composition of fine and coarse particles in relation with the Asian Dust events, Atmos. Environ., 37, 753–765, doi:10.1016/S1352-2310(02)00954-8, 2003.

Kim, S.-W., Yoon, S.-C., Jefferson, A., Ogren, J. A., Dutton, E. G., Won, J.-G., Ghim, Y. S., Lee, B.-I., and Han, J.-S.: Aerosol optical, chemical and physical properties at Gosan, Korea during Asian dust and pollution episodes in 2001, Atmos. Environ., 39, 39–50, doi:10.1016/j.atmosenv.2004.09.056, 2005.

Kim, S.-W., Yoon, S.-C., Kim, J., Kang, J.-Y., and Sugimoto, N.: Asian dust event observed in Seoul, Korea, during 29–31 May 2008: Analysis of transport and vertical distribution of dust particles from lidar and surface measurements, Sci. Total Environ., 408, 1707–1718, doi:10.1016/j.scitotenv.2009.12.018, 2010.

Kwon, H.-J., Cho, S.-H., Chun, Y., Lagarde, F., and Pershagen, G.: Effects of the Asian Dust events on daily mortality in Seoul, Korea, Environ. Res., 90, 1–5, doi:10.1006/enrs.2002.4377, 2002.

Lee, B.-K., Jun, N.-Y., and Lee, H. K.: Comparison of particulate matter characteristics before, during, and after Asian dust events in Incheon and Ulsan, Korea, Atmos. Environ., 38, 1535–1545, doi:10.1016/j.atmosenv.2003.12.021, 2004.

Lee, D. G., Lee, Y.-M., Jang, K.-W., Yoo, C., Kang, K.-H., Lee, J.-H., Jung, S.-W., Park, J.-M., Lee, S.-B., Han, J.-S., Hong, J.-H., and Lee, S.-J.: Korean national emissions inventory system and 2007 air pollutant emissions, Asian, J. Atmos. Environ., 5, 278–291, doi:10.5572/ajae.2011.5.4.278, 2011.

Lee, J., Kim, J., Song, C. H., Ryu, J.-H., Ahn, Y.-H., and Song, C. K.: Algorithm for retreval of aerosol optical properties over the ocean from the Geostationary Ocean Color Imager, Remote Sens. Environ., 114, 1077–1088, doi:10.1016/j.rse.2009.12.021, 2010.

Lee, S.-H., Lee, H. W., Kim, Y.-K., Jeon, W.-B., Choi, H.-J., and Kim, D.-H.: Impact of continuously varied SST on land-sea breezes and ozone concentration over south-western coast of Korea, Atmos. Environ., 45, 6439–6450, doi:10.1016/j.atmosenv.2011.07.059, 2011.

Li, M., Zhang, Q., Kurokawa, J., Woo, J.-H., He, K. B., Lu, Z., Ohara, T., Song, Y., Streets, D. G., Carmichael, G. R., Cheng, Y. F., Hong, C. P., Huo, H., Jiang, X. J., Kang, S. C., Liu, F., Su, H., and Zheng, B.: MIX: a mosaic Asian anthropogenic emission inventory for the MICS-Asia and the HTAP projects, Atmos. Chem. Phys. Discuss., 15, 34813–34869, doi:10.5194/acpd-15-34813-2015, 2015.

Li, X., Choi, Y., Czader, B., Roy, A., Kim, H., Lefer, B., and Pan, S.: The impact of observation nudging on simulated meteorology and ozone concentrations during DISCOVER-AQ 2013 Texas campaign, Atmos. Chem. Phys., 16, 3127–3144, doi:10.5194/acp-16-3127-2016, 2016.

Ngan, F., Byun, D., Kim, H., Lee, D., Rappengluck, B., and Pour-Biazar, A.: Performance assessment of retrospective meteorological inputs for use in air quality modeling during TexAQS 2006, Atmos. Environ., 54, 86–96, doi:10.1016/j.atmosenv.2012.01.035, 2012.

Nolte, C. G., Appel, K. W., Kelly, J. T., Bhave, P. V., Fahey, K. M., Collett Jr., J. L., Zhang, L., and Young, J. O.: Evaluation of the Community Multiscale Air Quality (CMAQ) model v5.0 against size-resolved measurements of inorganic particle composition across sites in North America, Geosci. Model Dev., 8, 2877–2892, doi:10.5194/gmd-8-2877-2015, 2015.

Otte, T. L.: The impact of nudging in the meteorological model for retrospective air quality simulations. Part I: Evaluation against national observation networks, J. Appl. Meteorol. Clim., 47, 1853–1867, doi:10.1175/2007JAMC1790.1, 2008a.

Otte, T. L.: The impact of nudging in the meteorological model for retrospective air quality simulations. Part II: Evaluating collocated meteorological and air quality observations, J. Appl. Meteorol. Clim., 47, 1868–1887, doi:10.1175/2007JAMC1791.1, 2008b.

Pai, P., Vijayaraghavan, K., and Seigneur, C.: Particulate matter modeling in the Los Angeles basin us-

ing SAQM-AERO, J. Air Waste Manage., 50, 32–42, doi:10.1080/10473289.2000.10463992, 2000.

Park, J. W., Lim, Y. H., Kyung, S. Y., An, C. H., Lee, S. P., Jeong, S. H., and Ju, Y.-S.: Effects of ambient particulate matter on peak expiratory flow rates and respiratory symptoms of asthmatics during Asian dust periods in Korea, Respirology, 10, 470–476, doi:10.1111/j.1440-1843.2005.00728.x, 2005.

Park, R. S., Song, C. H., Han, K. M., Park, M. E., Lee, S.-S., Kim, S.-B., and Shimizu, A.: A study on the aerosol optical properties over East Asia using a combination of CMAQ-simulated aerosol optical properties and remote-sensing data via a data assimilation technique, Atmos. Chem. Phys., 11, 12275–12296, doi:10.5194/acp-11-12275-2011, 2011.

Roy, B., Mathur, R., Gilliland, A. B., and Howard, S. C.: A comparison of CMAQ-based aerosol properties with IMPROVE, MODIS, and AERONET data, J. Geophys. Res., 112, D14301, doi:10.1029/2006JD008085, 2007.

Skamarock, W., Klemp, J. B., Dudhia, J., Gill, D. O., Barker, D. M., Duda, M. G., Huang, X.-Y., Wang, W., and Powers, J. G.: A description of the advanced research WRF version 3, NCAR technical note NCAR/TN/u2013475, 2008.

Song, C. H., Park, M. E., Lee, K. H., Ahn, H. J., Lee, Y., Kim, J. Y., Han, K. M., Kim, J., Ghim, Y. S., and Kim, Y. J.: An investigation into seasonal and regional aerosol characteristics in East Asia using model-predicted and remotely-sensed aerosol properties, Atmos. Chem. Phys., 8, 6627–6654, doi:10.5194/acp-8-6627-2008, 2008.

Stone, E. A., Yoon, S.-C., and Schauer, J. J.: Chemical characterization of fine and coarse particles in Gosan, Korea during springtime dust events, Aerosol Air Qual. Res., 11, 31–43, doi:10.4209/aaqr.2010.08.0069, 2011.

Tie, X., Geng, F., Peng, L., Gao, W., and Zhao, C.: Measurement and modeling of O_3 variability in Shanghai, China: Application of the WRF-Chem model, Atmos. Environ., 43, 4289–4302, doi:10.1016/j.atmosenv.2009.06.008, 2009.

Yarwood, G., Rao, S., Yocke, M., and Whitten, G.: Updates to the carbon bond chemical mechanism: CB05. Final report to the US EPA, RT-0400675, available at: http://www.camx.com/publ/pdfs/cb05_final_report_120805.pdf (last access: 10 September 2016), 2005.

Zhang, Q., Streets, D. G., Carmichael, G. R., He, K. B., Huo, H., Kannari, A., Klimont, Z., Park, I. S., Reddy, S., Fu, J. S., Chen, D., Duan, L., Lei, Y., Wang, L. T., and Yao, Z. L.: Asian emissions in 2006 for the NASA INTEX-B mission, Atmos. Chem. Phys., 9, 5131–5153, doi:10.5194/acp-9-5131-2009, 2009.

Zhao, B., Wang, P., Ma, J. Z., Zhu, S., Pozzer, A., and Li, W.: A high-resolution emission inventory of primary pollutants for the Huabei region, China, Atmos. Chem. Phys., 12, 481–501, doi:10.5194/acp-12-481-2012, 2012.